© AUG 2026 | IRE Journals | Volume 10 Issue 2 | ISSN: 2456-8880
DOI: https://doi.org/10.64388/IREV10I2-1722370

Comparative Study of Mixed Convection Effects on MHD Casson Dusty Two-Phase Flow over a Stretching Sheet

JYOTI D.K[1], DHANANJAIAH D.S[2], PRAKASHA. P[3]

[1]Department of Mathematics, Government College for Women (A), Mandya-571403, Karnataka, India.

[2]Department Of Mathematics, Government First Grade College, K.R. Nagara, Mysore-571602, Karnataka, India.

[3]Department Of Mathematics, Government First Grade College, Magadi- 562120, Karnataka, India.

Abstract- The present study investigates the nonlinear mixed convection flow and heat transfer characteristics of a magnetohydrodynamic (MHD) Casson dusty fluid over a stretching sheet in the presence of internal heat generation effects. The influences of space-dependent and temperature-dependent heat generation parameters are incorporated into the analysis. Using suitable similarity transformations, the governing nonlinear partial differential equations are converted into a system of ordinary differential equations and solved numerically using the Runge-Kutta-Fehlberg (RKF) method combined with the shooting technique. The analysis is performed for the parameter ranges $M = 0\text{-}1, \beta = 0.5\text{-}1.5, Qt = 0\text{-}0.4, Qe = 0\text{-}0.4$, with a comparative investigation between the absence ($\lambda = 0$) and presence ($\lambda = 0.5$) of mixed convection. The results show that increasing the Casson parameter significantly reduces the fluid velocity while enhancing the temperature distribution, whereas the magnetic parameter suppresses the momentum boundary layer because of the Lorentz force. Both space-dependent and temperature-dependent heat generation parameters increase the thermal boundary layer thickness. Furthermore, mixed convection enhances fluid motion and improves the local heat transfer rate compared with the $\lambda = 0$ case. The fluid-phase velocity and temperature are consistently higher than those of the dust phase over the entire parameter range considered. These findings provide useful insight into thermal transport and flow control in polymer extrusion, metallurgical processing, cooling of stretching surfaces, lubrication systems, and related heat-transfer devices.

Keywords: casson fluid, dusty: nonlinear thermal convection, mhd, irregular heat source.

I. INTRODUCTION

Convection phenomena involving the combined influence of externally driven flow and buoyancy-induced motion are commonly referred to as mixed convection. In such transport processes, fluid motion is governed simultaneously by external forcing mechanisms and density variations arising from temperature differences within the fluid. Mixed convection plays a significant role in many practical engineering systems, particularly in small-scale thermal devices and industrial applications such as solar energy collectors, cooling of electronic components, thermal energy storage systems, cryogenic engineering, and nuclear reactor technologies. Owing to its wide range of applications, considerable research attention has been devoted to the analysis of mixed convection flows under various physical conditions [1-8]. However, in several thermal systems, the conventional linear relationship between density and temperature may not accurately describe the transport behavior, especially when large temperature differences are involved. This limitation has motivated researchers to investigate nonlinear convection effects, where nonlinear temperature-dependent density variations substantially alter the momentum and heat transfer characteristics of the flow. Nonlinear convection has a significant impact on a number of manufacturing industries, particularly heat pumps, the combustion process, geothermal energy sources, the production of natural gas, refrigeration of electrical factors, medicinal products, etc. Due to this reason, Kameswaran et al. [9] analyzed boundary layer flow influenced by nonlinear convection and thermophoretic effects in a permeable medium over a vertical surface. Hayat et al. [10] studied the three-dimensional flow behavior of Sisko nanofluid under combined convection conditions over an elastic stretching surface in the presence of thermal and solutal buoyancy effects. Khan et al. [11] investigated nonlinear mixed convection flow of tangent hyperbolic nanofluid over an expanding surface considering entropy generation effects and reported that the fluid velocity increases with the nonlinear convection parameter. Furthermore, Irfan [12] investigated the nonlinear mixed convection flow of an MHD Carreau nanofluid considering variable thermophysical properties. Furthermore, the influence of nonlinear convection on flow and heat transfer under various physical conditions has also been explored by several authors including Idowu et al. [13], Ibrahim and Kenea [14], Kenea and Ibrahim [15], and Reddy et al. [16].

The study of non-Newtonian fluid flow has attracted considerable interest due to its important role in many engineering and industrial processes. Unlike Newtonian fluids, non-Newtonian fluids exhibit complex rheological characteristics such as variable viscosity, yield stress, and shear-dependent behavior. To describe these complex flow properties, several mathematical models have been proposed in the literature, including the Carreau-Yasuda, Casson, Cross, Maxwell, Powell-Eyring, Prandtl-Eyring, Ellis, Jeffery, and generalized power-law models [17-19]. These models have been widely utilized to analyze fluid transport phenomena under different physical conditions and geometrical configurations. Among the various non-Newtonian fluid models, the Casson fluid model introduced by Casson [20] in 1959 has received significant attention because of its ability to represent the behavior of yield stress fluids. The Casson model is particularly useful in describing the flow of suspensions, emulsions, biological fluids, and blood flow at low shear rates. Due to these characteristics, Casson fluids have numerous applications in biomedical engineering, food processing, cosmetic manufacturing, pharmaceutical industries, and petroleum engineering. Several investigations related to Casson fluid flow have been reported in recent years. Mukhopadhyay et al. [21] analyzed the unsteady two-dimensional flow of Casson fluid over a stretching surface with prescribed thermal conditions. Nandeppanavar et al. [22] examined the steady flow of Casson nanofluid over an exponentially stretching sheet and observed a reduction in fluid velocity with increasing Casson parameter values. Awais et al. [23] studied the effects of heat and mass transfer on MHD Casson fluid flow through a porous medium over a shrinking surface. In addition, numerous studies concerning Casson fluid and Casson nanofluid flow under different physical situations have been presented in Refs. [24-28].

Dusty fluid flow has attracted significant attention because of its important applications in engineering and industrial processes. A dusty fluid consists of a fluid containing suspended solid particles, where the interaction between the fluid and particle phases strongly influences the momentum and heat transfer characteristics. Such flows are encountered in combustion systems, aerosol transport, geothermal engineering, petroleum industries, nuclear reactors, and powder processing technologies. Owing to its practical importance, dusty fluid flow under various physical and thermal conditions has attracted considerable attention from researchers in recent years [29-35].

The investigation of nonlinear mixed convection in Casson dusty fluid flow over a stretching sheet has gained considerable importance because of its wide range of engineering and industrial applications. The interaction between the Casson fluid and suspended dust particles considerably influences the momentum and thermal transport characteristics, especially in the presence of magnetic field and internal heat generation effects. Such flow phenomena are frequently encountered in polymer extrusion, metallurgical processing, aerosol transport, geothermal engineering, cooling of continuous stretching surfaces, petroleum industries, nuclear reactor technology, and thermal energy systems. Although numerous studies have been reported on Casson fluid flow, dusty fluid transport, and mixed convection separately, very limited attention has been devoted to the comparative analysis of the presence and absence of mixed convection effects in MHD Casson dusty two-phase flow. In particular, the influence of nonlinear mixed convection on both fluid and dust phase characteristics has not been

© AUG 2026 | IRE Journals | Volume 10 Issue 2 | ISSN: 2456-8880
DOI: https://doi.org/10.64388/IREV10I2-1722370

adequately explored in the existing literature. Motivated by these practical applications and existing research gaps, the present work aims to investigate and compare the effects of mixed convection on the velocity and temperature distributions, skin-friction coefficient, and heat transfer characteristics of MHD Casson dusty fluid flow over a stretching sheet in the presence of temperature-dependent and space-dependent heat generation.

Mathematical formulation

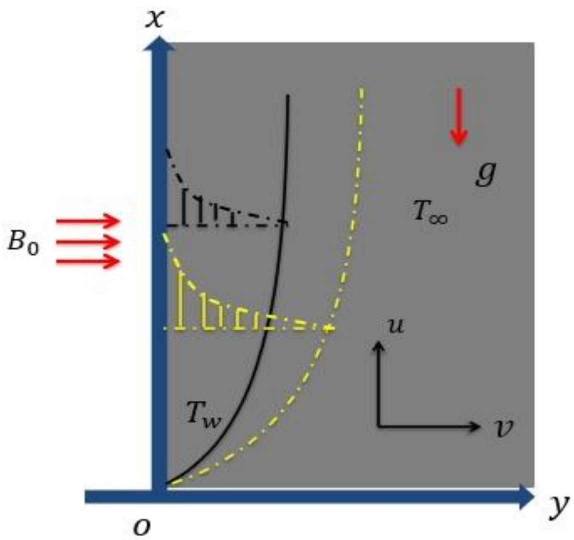

Fig 1: Schematic diagram of problem.

The present study examines the nonlinear mixed convection flow and heat transfer characteristics of an incompressible, electrically conducting Casson fluid containing suspended dust particles over a stretching sheet. The flow is assumed to be steady and laminar in nature. The stretching motion of the sheet is produced by applying two equal and opposite forces along the (x)-direction, causing the fluid motion to develop in the region (y>0). The sheet is stretched with the linear velocity (U_w (x)=bx), where (b) is a positive constant representing the stretching rate. In addition, a uniform transverse magnetic field of strength (B_0) is imposed normal to the flow direction along the (y)-axis. The effect of gravity is considered opposite to the direction of fluid motion in order to account for nonlinear mixed convection effects. The temperatures of the stretching surface and the ambient fluid are denoted by (T_f) and (T_∞), respectively. The simplified two-dimensional boundary layer equations of continuity, momentum and heat transport for both fluid phase and dust phase with usual notations are;

Casson Fluid Phase:

$$\frac{\partial u}{\partial x} + \frac{\partial v}{\partial y} = 0, \qquad (1)$$

$$u\frac{\partial u}{\partial x} + v\frac{\partial u}{\partial y} = \nu\left(1+\frac{1}{\beta}\right)\frac{\partial^2 u}{\partial y^2} + \frac{KN}{\rho}\left(u_p - u\right) + g\beta_0\left(T - T_\infty\right) + g\beta_1\left(T - T_\infty\right)^2 - \frac{\sigma B_0}{\rho} u \qquad (2)$$

$$\rho C_p\left(u\frac{\partial T}{\partial x} + v\frac{\partial T}{\partial y}\right) = k\frac{\partial^2 T}{\partial y^2} + \frac{\rho_p c_m}{\tau_T}\left(T_p - T\right) + Q_T\left(T - T_\infty\right) + Q_E\left(T_f - T_\infty\right)\exp\left(-n\sqrt{\frac{b}{\nu}}\,y\right), \qquad (3)$$

Dust Phase:

$$\frac{\partial u_p}{\partial x} + \frac{\partial v_p}{\partial y} = 0, \qquad (4)$$

$$u_p \frac{\partial u_p}{\partial x} + v_p \frac{\partial u_p}{\partial y} = \frac{KN}{\rho_p}(u - u_p), \tag{5}$$

$$\left(u_p \frac{\partial T_p}{\partial x} + v_p \frac{\partial T_p}{\partial y}\right) = \frac{1}{\tau_T}\left(T - T_p\right) \tag{6}$$

where x and y denote the cartesian co-ordinates, (u, v) and (u_p, v_p) are velocity components of fluid and dust phase along x and y directions respectively, β -Casson fluid parameter, ν -kinematic viscosity coefficient, ρ and ρ_p -density of the fluid and dust particle respectively, $K = 6\pi\mu r$ -strokes drag coefficient, N-number density of dust particles, μ dynamic viscosity of fluid, r radius of dust particle, k-thermal conductivity of the fluid, T_∞ -uniform ambient temperature, T and T_p -temperature of fluid and dust particle, Q_E -exponential heat source, Q_T -heat generation source, B_0 -Magnetic field, C_p-specific heat capacity at constant pressure, C_m -specific heat of dust particle, τT -relaxation time of the dust particle, σ-electrical conductivity, β_0 and β_1 -linear and nonlinear volumetric thermal expansion coefficient, g -acceleration due to gravity, respectively.

The relevant boundary conditions are;

$$u = U_w, v = 0, T = T_f \text{ at } y = 0,$$
$$u \to 0, u_p \to 0, v_p \to v, T \to T_\infty, T_p \to T_\infty \text{ as } y \to \infty. \tag{7}$$

Introduce the following similarity transformations;

$$u = bxf'(\xi),\ v = -\sqrt{vb}\, f(\xi),\ \xi = \sqrt{\frac{b}{v}}y,\ u_p = bxF'(\xi),\ v_p = -\sqrt{vb}\, F(\xi),$$

$$T = T_\infty + (T_f - T_\infty)\theta(\xi),\ \ T_p = T_\infty + (T_f - T_\infty)\theta_p(\xi) \tag{8}$$

Using the transformations (8), into equations (2),(3) and (5)-(7) yield;

$$\left(1 + \frac{1}{\beta}\right)f''' + ff'' - f'^2 + l\beta_v(F' - f') - Mf' + \lambda(\theta + \alpha\theta^2) = 0 \tag{9}$$

$$FF'' - (F')^2 + \beta_v(f' - F') = 0, \tag{10}$$

The term $F\,F'' - (F')^2$ in Equation (10) arises directly from the similarity transformation of the dust-phase momentum equation (5) using the velocity transformations defined in Equation (8).

$$\theta'' + Prf\theta' + l\gamma\beta_t Pr(\theta_p - \theta) + PrQ_t\theta + PrQ_e\, exp(-\xi n) = 0, \tag{11}$$

$$\theta_p{}'F - \beta_t(\theta_p - \theta) = 0. \tag{12}$$

During the nondimensionalization process, the transformed energy equation is divided by $\rho Cp\, b\left(T_f - T_\infty\right)$, whereby the factor $(T_f - T_\infty)$ is absorbed into the dimensionless heat source parameters Qt and Qe, leading to the exponential heat source term $Qe\, exp(-n\xi)$ in equation (11).

Reduced boundary conditions are;

$$f(\xi) = 0,\ f'(\xi) = 1,\ \theta(\xi) = 1 \text{ At } \xi = 0,$$

$$F'(\xi) \to 0,\ f'(\xi) \to 0,\quad F(\xi) \to f(\xi),\ \theta(\xi) \to 0,\ \theta_p(\xi) \to 0 \text{ As } \xi \to \infty, \tag{12}$$

where β is the Casson fluid parameter, M is the magnetic parameter, l is the mass concentration of dust particles, β_v is the fluid-particle interaction parameter for velocity, λ is the mixed convection parameter, α is the nonlinear convection parameter, Pr is the Prandtl number, β_t is the fluid–particle interaction parameter for temperature, Qt is the temperature-dependent heat source parameter, and Qe is the exponential heat source parameter. These parameters are defined as

$$l = \frac{KN}{\rho},$$

$$\beta_v = \frac{1}{b\tau_v}, \tau_v = \frac{m}{K}, Re_x = \frac{U_w x}{\nu} = \frac{bx^2}{\nu},$$

$$\gamma = \frac{Cm}{C_p},$$

$$\lambda = \frac{Gr}{Rex^2}, Gr = \frac{g\beta_0(T_f - T_\infty)x^3}{\nu^2},$$

$$\alpha = \frac{\beta_1(T_f - T_\infty)}{\beta_0},$$

$$Pr = \frac{\mu C_p}{k}, \beta_t = \frac{1}{b\tau_t},$$

$$Qt = \frac{Q_T}{\rho Cpb},$$

$Qe = \frac{Q_E}{\rho C_p b}$.

The skin friction coefficient and Nusselt number in non-dimensional form are

$$\sqrt{Re_x}C_f = \left(1+\frac{1}{\beta}\right)f''(0), \quad (14)$$

$$\frac{Nu}{\sqrt{Re_x}} = -\theta'(0), \quad (15)$$

Numerical Solution Procedure

The highly nonlinear coupled ordinary differential equations (9)-(12), together with the associated boundary conditions, are solved numerically using the shooting technique in combination with the RKF method. For this purpose, the governing higher-order differential equations are first transformed into a system of first-order ordinary differential equations by introducing the following variables: Set

$x_1 = f,\ x_2 = f',\ x_3 = f'',\ x_4 = F,\ x_5 = F'$

$x_6 = \theta \quad x_7 = \theta'$ and $x_8 = \theta_p$ Accordingly, we have;

$$x_1' = x_2 \quad (16)$$

$$x_2' = x_3 \quad (17)$$

$$x_3' = [\beta/(1+\beta)]\,[x_2^2 - x_1x_3 - l\beta_v(x_5 - x_2) + Mx_2 - \lambda(x_6 + \alpha x_6^2)] \quad (18)$$

$$x_4' = x_5 \quad (19)$$

$$x_5' = (1/x_4)\,[x_5^2 - \beta_v(x_2 - x_5)] \quad (20)$$

$$x_6' = x_7 \quad (21)$$

$$x_7' = -Prx_1x_7 - l\gamma\beta_t Pr(x_8 - x_6) - PrQ_t x_6 - PrQ_e\, exp(-\xi n) \quad (22)$$

$$x_8' = [\beta_t/x_4]\,(x_8 - x_6) \quad (23)$$

It is observed that Equations (20) and (23) contain the terms $1/x_4$, where $x_4 = F$. An apparent singularity may arise if F becomes zero during the numerical integration. In the present computation, this difficulty is avoided by treating the unknown initial value $m_2 = F(0)$ as a non-zero shooting parameter, which is determined iteratively together with the other unknown initial conditions. Consequently, x_4 remains finite throughout the computational domain, and the terms involving $1/x_4$ do not produce numerical singularities. The convergence of the solution was verified by reducing the step size and tightening the convergence tolerance, and no significant variation was observed in the computed results.

The transformed boundary conditions for the first-order system are expressed as

© AUG 2026 | IRE Journals | Volume 10 Issue 2 | ISSN: 2456-8880
DOI: https://doi.org/10.64388/IREV10I2-1722370

$$x_1(0) = 0,\ x_2(0) = 1, \quad x_3(0) = m_1, \quad x_4(0) = m_2,$$
$$x_5(0) = m_3, \quad x_6(0) = 1, \quad x_7(0) = m_4, \quad x_8(0) = m_5. \tag{24}$$

Here, $m_1, m_2, m_3, m_4,$ and m_5 denote the unknown initial conditions associated with the missing boundary values. These quantities are determined iteratively using the shooting technique so that the asymptotic boundary conditions are satisfied accurately. The resulting system of initial value problems is then integrated numerically using the RKF method. In the computations, the convergence criterion is taken as 10^{-6}, while the step size is fixed as $\Delta\eta = 0.001$. The accuracy of the present numerical method is verified by comparing the local Nusselt number obtained from the present computation with the previously published results of Grubka and Bobba [36] and Abel and Mahesha [37] for the limiting case $M = 0, \lambda = 0, \beta \rightarrow \infty, l = 0,$ and $Qe = Qt = 0$. The comparison presented in Table 1 shows excellent agreement between the present results and the available literature. The close correspondence of the numerical values confirms the accuracy and reliability of the present RKF shooting method for solving the transformed boundary-layer equations.

Table 1: Comparison of the local Nusselt number for the limiting case

$M = 0, \lambda = 0, \beta \rightarrow \infty, l = 0,$ and $Q_e = Q_t = 0$.

Pr	Grubka and Bobba [36]	Abel and Mahesha [37]	Present study
0.72	1.0885	1.0885	1.0885
1.0	1.3333	1.3333	1.3333
10	4.7969	4.7968	4.7968

II. RESULTS AND DISCUSSION

The effects of the governing physical parameters on the velocity and temperature distributions are analyzed graphically, while the variations in the skin-friction coefficient and local Nusselt number are presented in tabular form. The influence of the fluid-particle interaction parameters Casson fluid parameter (β), nonlinear convection parameter (α), magnetic parameter (M), volumetric heat generation parameter (Q_t), and exponential heat generation parameter (Q_e) are discussed in detail. Unless otherwise specified, the computations are carried out for the fixed values

($\beta = 1.5$), ($\beta_t = \beta_v = 0.8$), ($Q_e = Q_t = 0.2$), ($l = 0.6$), ($Pr = 6.2$), $(M = 0.5)$ and $(\alpha = 0.5)$. Figure 2 present the influence of the Casson fluid parameter (β) on the velocity and temperature distributions of both fluid and dust phases in the presence $(\lambda = 0.5)$ and absence ($\lambda = 0$) of mixed convection effects. It is observed from the velocity profiles that increasing the Casson parameter reduces the fluid velocity in both phases. Physically, larger values of (β) enhance the yield stress of the Casson fluid, which strengthens the resistance to fluid motion and consequently suppresses the momentum boundary layer development. A comparison between the cases ($\lambda = 0.5$) and ($\lambda = 0$) reveals that the velocity profiles are comparatively higher in the presence of mixed convection. This behavior occurs because the buoyancy force generated by mixed convection assists the fluid motion and partially overcomes the resistive effect caused by the Casson parameter. In contrast, in the absence of mixed convection ($\lambda = 0$), the velocity decays more rapidly due to the lack of buoyancy assistance. The effects of the Casson parameter on the temperature distributions for both fluid and dust phases are displayed in figure 3. It is noticed that the temperature profiles increase with increasing values of (β). The enhancement in temperature is attributed to the increase in fluid resistance, which weakens the fluid motion and reduces the rate of heat transport away from the surface. As a result, thermal energy accumulates within the boundary layer region, leading to higher temperatures and thicker thermal boundary layers. Moreover, the temperature profiles corresponding to ($\lambda = 0$) are found to be higher than those for ($\lambda = 0.5$). The presence of mixed convection strengthens the fluid motion and improves convective heat transport, thereby reducing the thermal boundary layer thickness. Consequently, the fluid temperature decreases in the presence of mixed convection compared to the pure forced convection case.

Figure 4 presents the effect of the nonlinear convection parameter (α) on the velocity and temperature distributions. An increase in the nonlinear convection parameter strengthens the buoyancy force, which accelerates the fluid flow and enlarges the momentum boundary layer thickness. On the other hand, the temperature profile decreases due to the enhanced convection mechanism, which transports thermal energy away from the surface more effectively. The influence of the magnetic parameter (M) on the dimensionless velocity profiles of both fluid and dust phases is displayed in figure 5. It is evident that increasing the magnetic parameter significantly reduces the velocity distribution. Physically, the applied magnetic field generates a Lorentz force that opposes the fluid motion, resulting in a deceleration of the flow and a thinner momentum boundary layer. Figures 6 and 7 depict the effects of the exponential heat generation parameter (Q_e) and volumetric heat generation parameter (Q_t) on the temperature distributions for both fluid and dust phases in the presence ($\lambda = 0.5$) and absence ($\lambda = 0$) of mixed convection effects. It is observed that the temperature profiles increase substantially with increasing values of (Q_e) and (Q_t). Physically, larger heat generation parameters introduce additional thermal energy into the fluid domain, which increases the internal energy of the system. As a result, the thermal boundary layer becomes thicker and the temperature of both phases rises considerably. Furthermore, the stronger heat generation mechanism weakens the rate of heat dissipation from the surface, leading to an overall enhancement in the thermal field. A comparison between the mixed convection case ($\lambda = 0.5$) and the non-mixed convection case ($\lambda = 0$) indicates that the temperature profiles are comparatively lower in the presence of mixed convection. This reduction in temperature occurs because the buoyancy force associated with mixed convection enhances the fluid motion and improves the convective transport of heat away from the surface. As a result, the thermal boundary layer thickness decreases when mixed convection effects are present.

Overall, the presence of mixed convection ($\lambda = 0.5$) significantly enhances the fluid motion due to the action of buoyancy forces, resulting in higher velocity distributions for both fluid and dust phases when compared with the absence of mixed convection ($\lambda = 0$). The enhanced convection mechanism accelerates the flow and increases the momentum boundary layer thickness. Conversely, the temperature distributions are found to be lower in the presence of mixed convection because the stronger fluid motion improves convective heat transport from the surface to the ambient fluid. In contrast, when mixed convection effects are absent ($\lambda = 0$), the fluid velocity decreases while the temperature profiles become comparatively higher due to weaker convective cooling. Therefore, it can be concluded that mixed convection assists the momentum transport while suppressing the thermal boundary layer thickness in both fluid and dust phases.

Tables 2-7 demonstrate the effects of the parameter β, M, Q_e, Q_t and α on the skin-friction coefficient $(C_f Re_x^{1/2})$ and local Nusselt number $(Nu_x Re_x^{-1/2})$ in the presence ($\lambda = 0.5$) and absence ($\lambda = 0$) of mixed convection. It is observed that increasing values of β reduce both the skin-friction coefficient and heat transfer rate due to the enhanced resistance offered by the Casson fluid. The magnetic parameter increases the magnitude of the skin-friction coefficient while reducing the local Nusselt number because the Lorentz force opposes the fluid motion and weakens heat transfer. Furthermore, the negative values of the skin-friction coefficient observed in the tables are a consequence of the chosen stretching-sheet coordinate convention and indicate that the wall shear stress acts opposite to the stretching direction. Increasing values of the heat generation parameters Q_e and Q_t significantly decrease the local Nusselt number by supplying additional thermal energy to the

© AUG 2026 | IRE Journals | Volume 10 Issue 2 | ISSN: 2456-8880
DOI: https://doi.org/10.64388/IREV10I2-1722370

fluid system, which thickens the thermal boundary layer and weakens the surface temperature gradient. For larger values of Q_e and Q_t, negative values of the Nusselt number are observed, indicating reverse heat transfer behavior. It is also observed that the skin-friction coefficient remains unchanged for all values of Q_e and Q_t, when λ=0 because the buoyancy term vanishes, making the momentum equation independent of the thermal field. Furthermore, the nonlinear convection parameter α considerably enhances both the skin-friction coefficient and local Nusselt number in the mixed convection case due to stronger buoyancy effects. The relatively large values α= 50 and 100 are considered to represent strong nonlinear buoyancy effects that may occur in high-temperature thermal processing and metallurgical applications. Overall, the presence of mixed convection improves the momentum and thermal transport characteristics compared to the absence of mixed convection.

Table 2: Variations in the skin friction coefficient and local Nusselt number for different values of the Casson fluid parameter (β) in the presence (λ=0.5) and absence (λ=0) of convection parameter.

β	$\lambda = 0.5$ $C_f Re_x^{1/2}$	$\lambda = 0.5$ $Nu_x Re_x^{-1/2}$	$\lambda = 0$ $C_f Re_x^{1/2}$	$\lambda = 0$ $Nu_x Re_x^{-1/2}$
0.5	-1.94952	0.870549	-2.31717	0.80921
1.0	-1.52633	0.769039	-1.89039	0.66050
1.5	-1.36378	0.719227	-1.72543	0.57801

Table 3: Variations in the skin friction coefficient and local Nusselt number for different values of the magnetic parameter (M) in the presence (λ=0.5) and absence (λ=0) of convection parameter.

M	$\lambda = 0.5$ $C_f Re_x^{1/2}$	$\lambda = 0.5$ $Nu_x Re_x^{-1/2}$	$\lambda = 0$ $C_f Re_x^{1/2}$	$\lambda = 0$ $Nu_x Re_x^{-1/2}$
0	-1.10907	0.830795	-1.46524	0.71774
0.5	-1.36378	0.719227	-1.72543	0.57801
1.0	-1.58676	0.616387	-1.95186	0.44684

Table 5: Variations in the skin friction coefficient and local Nusselt number for different values of the exponential heat source (Q_e) in the presence (λ=0.5) and absence (λ=0) of convection parameter.

Q_e	$\lambda = 0.5$ $C_f Re_x^{1/2}$	$\lambda = 0.5$ $Nu_x Re_x^{-1/2}$	$\lambda = 0$ $C_f Re_x^{1/2}$	$\lambda = 0$ $Nu_x Re_x^{-1/2}$
0	-1.51060	1.749694	-1.72543	1.72830
0.2	-1.36378	0.719227	-1.72543	0.57801
0.4	-1.21287	-0.21116	-1.72543	-0.57228

© AUG 2026 | IRE Journals | Volume 10 Issue 2 | ISSN: 2456-8880
DOI: https://doi.org/10.64388/IREV10I2-1722370

Table 6: Variations in the skin friction coefficient and local Nusselt number for different values of the heat source (Q_t) in the presence (λ=0.5) and absence (λ=0) of convection parameter.

Q_t	$\lambda = 0.5$ $C_f Re_x^{1/2}$	$\lambda = 0.5$ $Nu_x Re_x^{-1/2}$	$\lambda = 0$ $C_f Re_x^{1/2}$	$\lambda = 0$ $Nu_x Re_x^{-1/2}$
0	-1.42047	1.251700	-1.72543	1.18766
0.2	-1.36378	0.719227	-1.72543	0.57801
0.4	-1.27130	-0.01305	-1.72543	-0.40936

Table 7: Variations in the skin friction coefficient and local Nusselt number for different values of the nonlinear convection parameter (α) in the presence (λ=0.5) and absence (λ=0) of convection parameter.

α	$\lambda = 0.5$ $C_f Re_x^{1/2}$	$\lambda = 0.5$ $Nu_x Re_x^{-1/2}$	$\lambda = 0$ $C_f Re_x^{1/2}$	$\lambda = 0$ $Nu_x Re_x^{-1/2}$
0.9	-1.36378	0.719227	-1.72543	0.57801
50	3.702438	1.291746	-1.72543	0.57801
100	7.701009	1.525003	-1.72543	0.57801

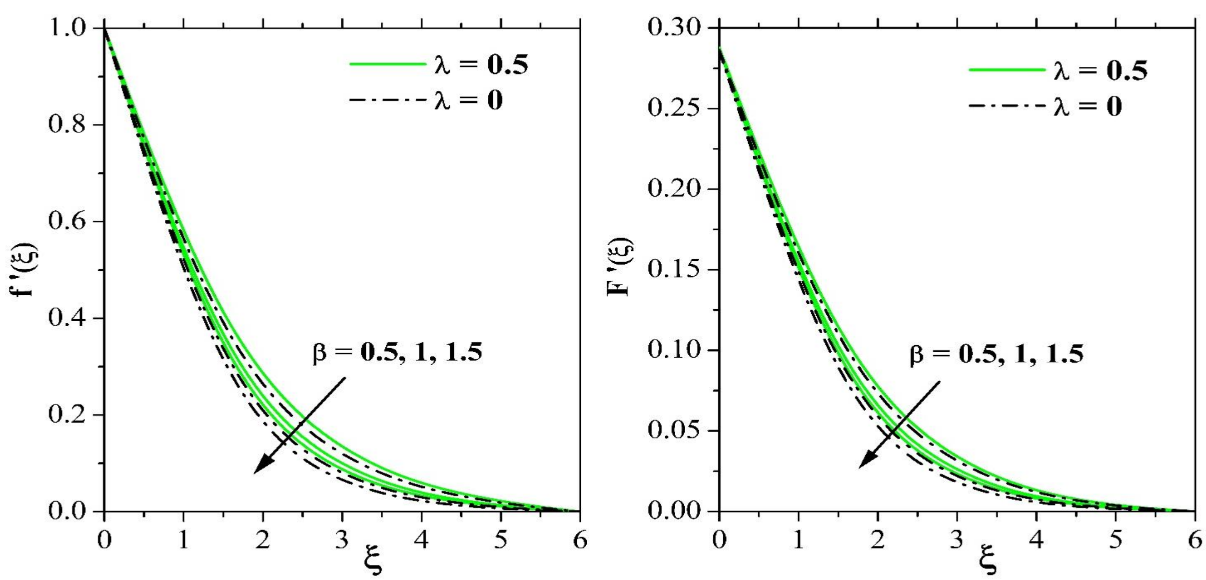

Figure 2: Influence of the Casson fluid parameter (β) on the velocity distributions of the fluid phase $f'(\xi)$ and dust phase $f'(\xi)$

© AUG 2026 | IRE Journals | Volume 10 Issue 2 | ISSN: 2456-8880
DOI: https://doi.org/10.64388/IREV10I2-1722370

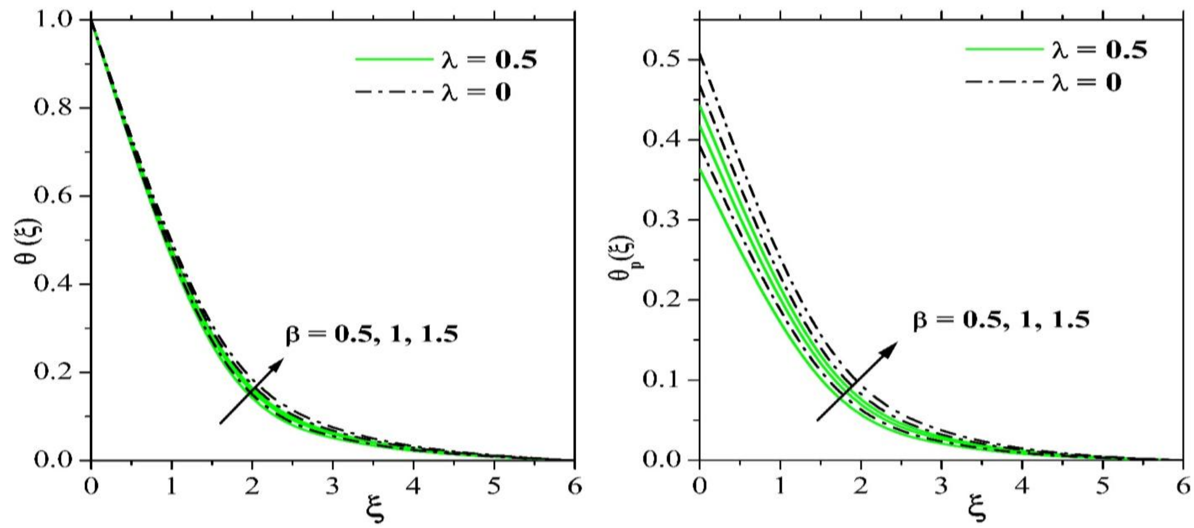

Figure 3: Influence of the Casson fluid parameter (β) on the temperature distributions of the fluid phase $\theta(\xi)$ and dust phase $\theta_p(\xi)$.

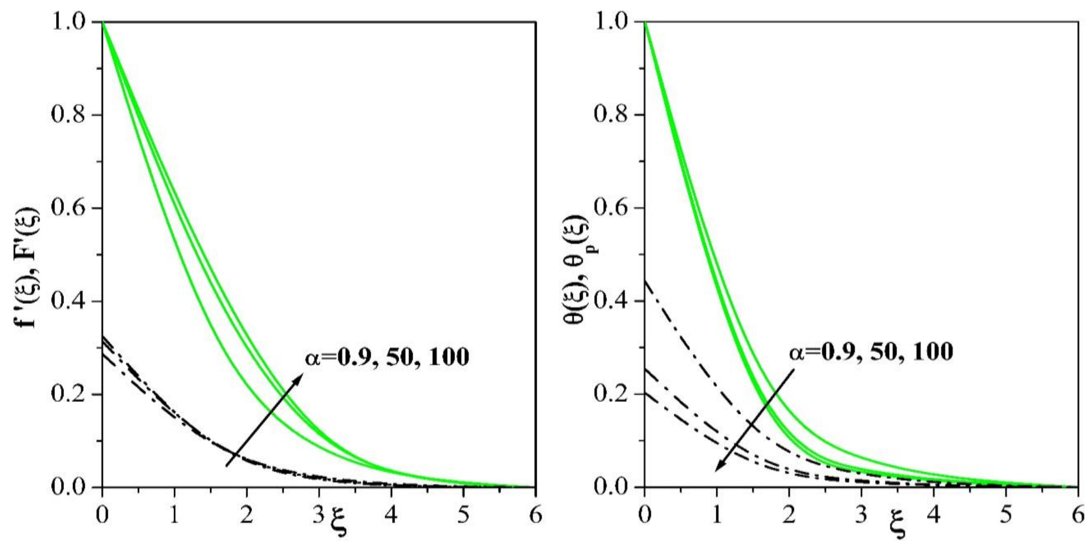

Figure 4: Influence of the nonlinear convection (α) on the velocity and temperature distributions of the fluid phase and dust phase.

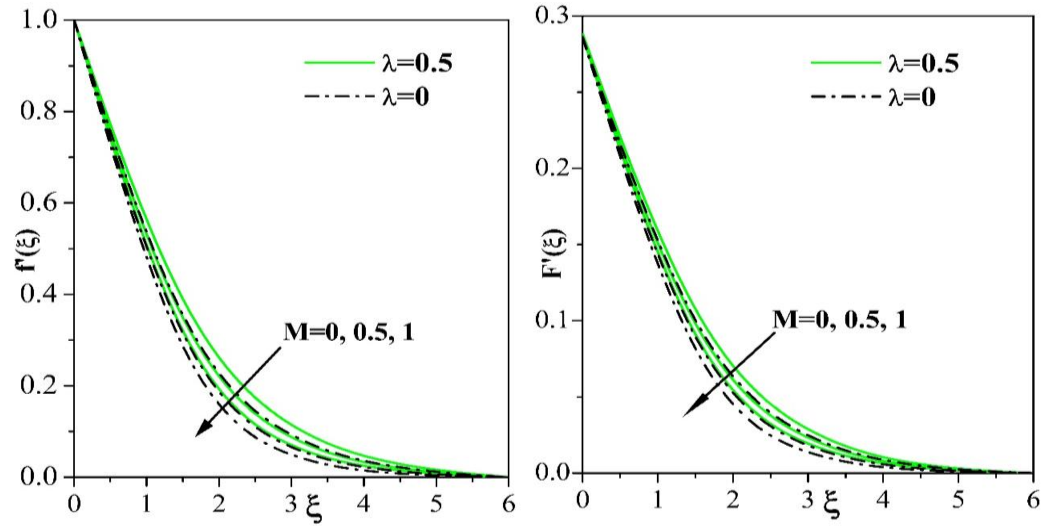

Figure 5: Influence of the magnetic parameter (M) on the velocity distributions of the fluid phase $f'(\xi)$and dust phase $F'(\xi)$.

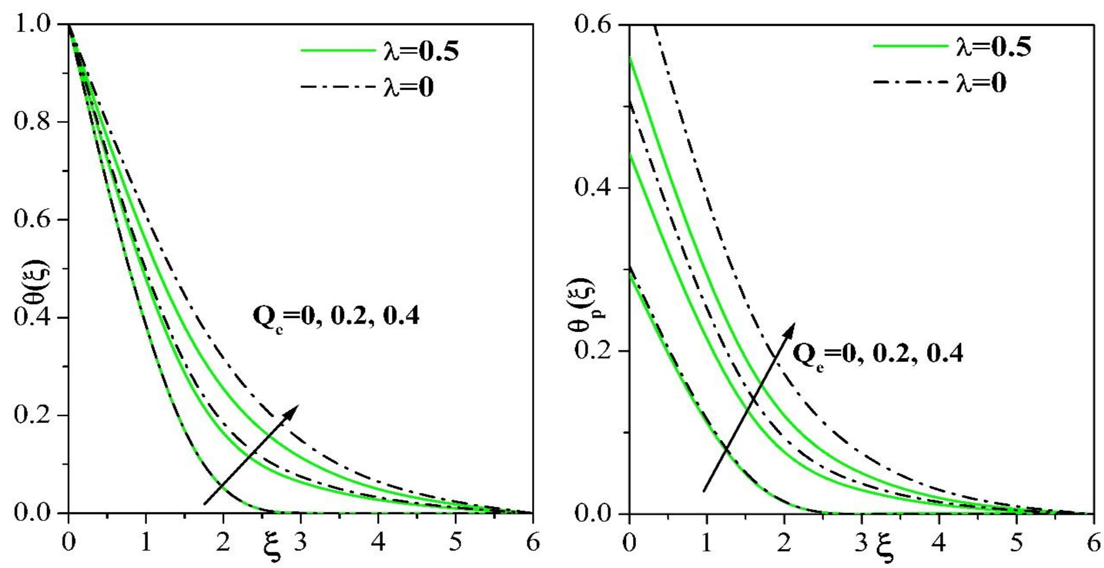

Figure 6: Influence of the exponential heat source (Q_e) on the temperature distributions of the fluid phase $\theta(\xi)$ and dust phase $\theta_p(\xi)$

© AUG 2026 | IRE Journals | Volume 10 Issue 2 | ISSN: 2456-8880
DOI: https://doi.org/10.64388/IREV10I2-1722370

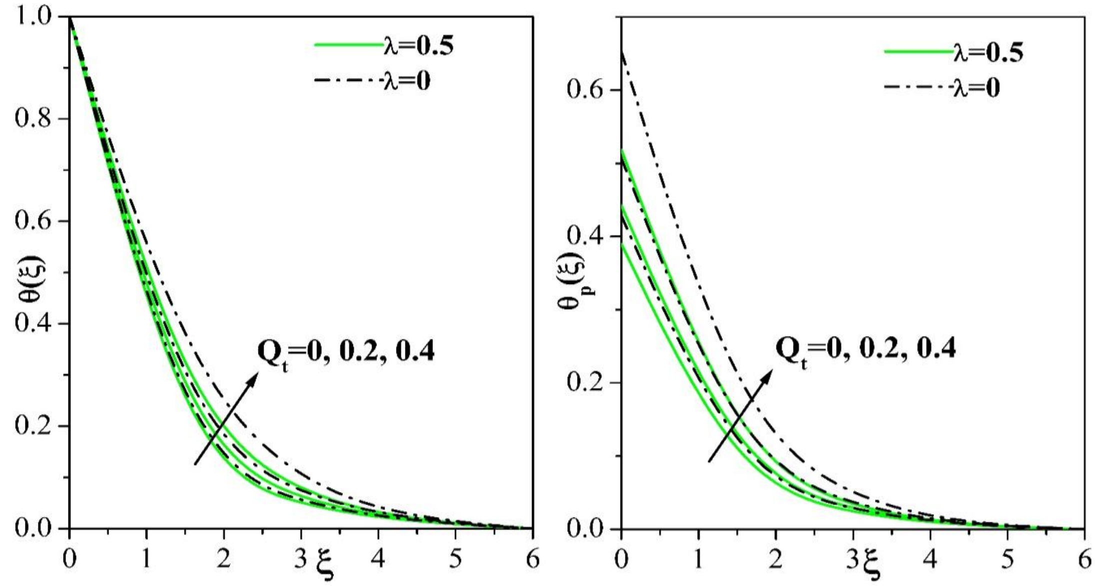

Figure 7: Influence of the heat source parameter (Q_t) on the temperature distributions of the fluid phase $\theta(\xi)$ and dust phase $\theta_p(\xi)$.

III. CONCLUDING REMARKS

In the present study, the effects of nonlinear convection on the flow and heat transfer characteristics of a Casson fluid over a stretching sheet have been investigated numerically in the presence of magnetic field and internal heat generation effects. The obtained results indicate that increasing values of the Casson fluid parameter reduce the velocity profiles while enhancing the temperature distributions due to the increase in fluid resistance. The magnetic parameter suppresses the fluid motion because of the opposing Lorentz force, whereas the heat generation parameters significantly increase the thermal boundary layer thickness by supplying additional thermal energy to the fluid system. Moreover, the nonlinear convection parameter enhances both the momentum and heat transfer characteristics due to stronger buoyancy effects. A comparative analysis between the presence ($\lambda = 0.5$) and absence ($\lambda = 0$) of mixed convection reveals that mixed convection improves the fluid motion and reduces the temperature distributions through enhanced convective cooling. Overall, the present investigation provides valuable insight into the transport phenomena of Casson fluid flow over a stretching sheet under mixed convection conditions. The outcomes of this study may be useful in various engineering and industrial applications such as polymer extrusion processes, cooling of stretching surfaces, metallurgical processes, lubrication technologies, thermal processing systems, and other heat transfer devices where efficient thermal management and flow regulation are essential.

REFERENCES

[1] Reddy Gorla, R. S., & Sidawi, I. (1994). Free convection on a vertical stretching surface with suction and blowing. Applied scientific research, 52(3), 247-257.

[2] Chamkha, A. J. (1997). Non-Darcy fully developed mixed convection in a porous medium channel with heat generation/absorption and hydromagnetic effects. Numerical Heat Transfer, Part A Applications, 32(6), 653-675.

[3] Hayat, T., Abbas, Z., Pop, I., & Asghar, S. (2010). Effects of radiation and magnetic field on the mixed convection stagnation-point flow over a vertical stretching sheet in a porous medium. International Journal of Heat and Mass Transfer, 53(1-3), 466-474.

[4] Das, K. (2013). Mixed convection stagnation point flow and heat transfer of Cu-water nanofluids towards a shrinking sheet. Heat Transfer—Asian Research, 42(3), 230-242.

[5] Islam, S., Khan, A., Kumam, P., Alrabaiah, H., Shah, Z., Khan, W., ... & Jawad, M. (2020). Radiative mixed convection flow of maxwell nanofluid over a stretching cylinder with joule heating and heat source/sink effects. Scientific reports, 10(1), 17823.

[6] Tulu, A., Hirpho, M., & Sohail, M. (2024). Modeling and simulation of mixed convection flow with viscous dissipation in a lid-driven hexagonal cavity using finite element method. International Journal of Thermofluids, 22, 100702.

[7] Al-Kaby, R. N., Abdulhaleem, S. M., Hameed, R. H., & Yasiry, A. (2025). Mixed convection heat transfer and fluid flow of nanofluid/porous medium under magnetic field influence. Applied Sciences, 15(3), 1087.

[8] Znaidia, S., Rehman, S., Drissi, N., Asiri, F., & Nasr, S. (2025). Mixed Convection Flow and Heat Transfer of Williamson Drilling Nanofluid Over a Stretching Cylinder Using Brinkman-Maxwell-Garnett Model and temperature-dependent Features. Journal of Nonlinear Mathematical Physics, 32(1), 78.

[9] Kameswaran, P. K., Sibanda, P., Partha, M. K., & Murthy, P. V. S. N. (2014). Thermophoretic and nonlinear convection in non-Darcy porous medium. Journal of Heat Transfer, 136(4), 042601.

[10] Hayat, T., Ullah, I., Alsaedi, A., Waqas, M., & Ahmad, B. (2017). Three-dimensional mixed convection flow of Sisko nanoliquid. International Journal of Mechanical Sciences, 133, 273-282.

[11] Khan, M. I., Khan, T. A., Qayyum, S., Hayat, T., Khan, M. I., & Alsaedi, A. J. T. E. P. J. P. (2018). Entropy generation optimization and activation energy in nonlinear mixed convection flow of a tangent hyperbolic nanofluid. The European Physical Journal Plus, 133(8), 329.

[12] Irfan, M. (2021). Study of Brownian motion and thermophoretic diffusion on non-linear mixed convection flow of Carreau nanofluid subject to variable properties. Surfaces and Interfaces, 23, 100926.

[13] Idowu, A. S., Akolade, M. T., Oyekunle, T. L., & Abubakar, J. U. (2021). Nonlinear convection flow of dissipative Casson nanofluid through an inclined annular microchannel with a porous medium. Heat transfer, 50(4), 3388-3406.

[14] Ibrahim, W., & Kenea, G. (2024). Nonlinear convection flow of a micropolar nanofluid past a stretching sphere with convective heat transfer. Journal of Nanofluids, 13(2), 407-422.

[15] Kenea, G., & Ibrahim, W. (2024). Nonlinear convection stagnation point flow of Oldroyd-B nanofluid with non-Fourier heat and non-Fick's mass flux over a spinning sphere. Scientific Reports, 14(1), 841.

[16] Reddy, G. S. K., Raju, S. S. K., Mulki, H., & Souayeh, B. (2026). Nonlinear Convection of a Power-Law Fluid-Saturated Reactive Porous Layer. Axioms, 15(7), 487.

[17] Ireka, I. E. (2015). Computational analysis of non-isothermal flow of non-Newtonian fluids.

[18] Fatahian, E., Kordani, N., & Fatahian, H. (2018). The application of computational fluid dynamics (CFD) method and several rheological models of blood flow: A review. Gazi University Journal of Science, 31(4), 1213–1227.

[19] Fatahian, E., Kordani, N., & Fatahian, H. (2018). A review on rheology of non-Newtonian properties of blood. IIUM Engineering Journal, 19(1), 237–250.

[20] Casson, N. (1959). Flow equation for pigment-oil suspensions of the printing ink-type. In C. C. Mill (Ed.), Rheology of disperse systems (pp. 84–104). Pergamon Press.

[21] Mukhopadhyay, S., De, P. R., Bhattacharyya, K., & Layek, G. C. (2013). Casson fluid flow over an unsteady stretching surface. Ain Shams Engineering Journal, 4(4), 933–938.

[22] Nandeppanavar, M. M., Vaishali, S., Kemparaju, M., & Raveendra, N. (2020). Theoretical analysis of thermal characteristics of Casson nanofluid flow past an exponential

stretching sheet in Darcy porous media. Case Studies in Thermal Engineering, 21, 100717.

[23] Awais, M., Raja, M. A. Z., Awan, S. E., Shoaib, M., & Ali, H. M. (2021). Heat and mass transfer phenomenon for the dynamics of Casson fluid through porous medium over shrinking wall subject to Lorentz force and heat source/sink. Alexandria Engineering Journal, 60(1), 1355–1363.

[24] Walelign, T., Haile, E., Kebede, T., & Walelgn, A. (2020). Analytical study of heat and mass transfer in MHD flow of chemically reactive and thermally radiative Casson nanofluid over an inclined stretching cylinder. Journal of Physics Communications, 4(12), 125003.

[25] Abo-Dahab, S., Abdelhafez, M., Mebarek-Oudina, F., & Bilal, S. (2021). MHD Casson nanofluid flow over nonlinearly heated porous medium in presence of extending surface effect with suction/injection. Indian Journal of Physics, 96(5), 1301–1315.

[26] Reddy, B. N., & Maddileti, P. (2023). Casson nanofluid and Joule parameter effects on variable radiative flow of MHD stretching sheet. Partial Differential Equations in Applied Mathematics, 7, 100487.

[27] Gubena, T., & Ibrahim, W. (2023). A 3D flow analysis of Casson nanofluid flow over a stretching surface with non-Fourier heat and non-Fick's mass flux. International Journal of Thermofluids, 20, 100488.

[28] Ali, M. Y., Reza-E-Rabbi, S., Ahmmed, S. F., Nabi, M. N., Azad, A. K., & Muyeen, S. (2024). Hydromagnetic flow of Casson nanofluid across a stretched sheet in the presence of thermoelectric and radiation effects. International Journal of Thermofluids, 21, 100484.

[29] Prakash, O. M., Makinde, O. D., Kumar, D., & Dwivedi, Y. K. (2015). Heat transfer to MHD oscillatory dusty fluid flow in a channel filled with a porous medium. Sadhana, 40(4), 1273-1282.

[30] Siddiqa, S., Begum, N., Hossain, M. A., Gorla, R. S. R., & Al-Rashed, A. A. (2018). Two-phase natural convection dusty nanofluid flow. International Journal of Heat and Mass Transfer, 118, 66-74.

[31] Reddy, M. G., Rani, M. S., Kumar, K. G., Prasannakumar, B. C., & Lokesh, H. J. (2020). Hybrid dusty fluid flow through a Cattaneo–Christov heat flux model. Physica A: Statistical Mechanics and its Applications, 551, 123975.

[32] Kalpana, G., & Saleem, S. (2022). Heat transfer of magnetohydrodynamic stratified dusty fluid flow through an inclined irregular porous channel. Nanomaterials, 12(19), 3309.

[33] Das, S., Sarkar, S., Ali, A., & Jana, R. N. (2024). Exploration of magnetically influenced flow dynamics of a dusty fluid induced by the ramped movement of a thermally active plate. Archive of Applied Mechanics, 94(2), 407-433.

[34] Alahmadi, H., Rauf, A., Mushtaq, T., Tanveer, N., Omar, M., & Shehzad, S. A. (2024). Time-dependent double phase dusty fluid flow over an oscillatory rotating disk. Heat Transfer, 53(3), 1336-1350.

[35] Kumar, M. D., Raju, C. S. K., Sajjan, K., Dharmaiah, G., Shah, N. A., & Yook, S. J. (2025). Deep neural network-based prediction and computational fluid dynamics analysis of convective heat transfer in dusty fluid flow over heated surface. Physics of Fluids, 37(2).

[36] Grubka, L.J. and Bobba, K.M., (1985). Heat transfer characteristics of a continuous, stretching surface with variable temperature.

[37] Abel, M.S. and Mahesha, N.J.A.M.M., (2008). Heat transfer in MHD viscoelastic fluid flow over a stretching sheet with variable thermal conductivity, non-uniform heat source and radiation. Applied Mathematical Modelling, 32(10), pp.1965-1983.